

that the light rays confined in a multimode waveguide strike the filter with angles ranging from  $\theta_0 - \theta_t$  to  $\theta_0 + \theta_t$  (2-dimensional light ray model), where  $\theta_0$  and  $\theta_t$  are the filter slanting angle and the maximum transmitting angle of the light rays to the waveguide axis, respectively. The apparent filter transmittance  $L(\lambda, \theta_0)$  is formulated as follows:

$$L(\lambda, \theta_0) = \frac{\sum_{p,s} \int_{-\theta_t}^{\theta_t} T(\lambda, \theta_0 + \theta) I(\theta) d\theta}{2 \int_{-\theta_t}^{\theta_t} I(\theta) d\theta} \quad (1)$$

where  $T(\lambda, \theta)$  is the filter transmittance for a collimated signal,  $\lambda$  is the wavelength and  $\theta$  the incident angle of the light, and  $I(\theta)$  is the angle distribution of the light rays transmitting in the waveguide. The indices  $p$  and  $s$  in the summation denote  $p$ - and  $s$ -polarisation, respectively.

We found the following new BPF configuration most suitable for multiplexing:

glass |HLH + (3HLHLHL3H)<sup>3</sup> + HLH| optical adhesive

where  $H$  and  $L$  stand for films of higher and lower refractive substances a quarter wavelength thick ( $\text{TiO}_2$  and  $\text{SiO}_2$ ), respectively. The bandwidth for 90% transmittance is as wide as 60 nm, in comparison with 50 nm or less by the conventional three-cavity BPF, HLHL + (LHLHLHLH)<sup>2</sup> + LHLH. The apparent bandwidth and the centre wavelength shifts of the filter derived from the formula almost agreed with the experimental results.

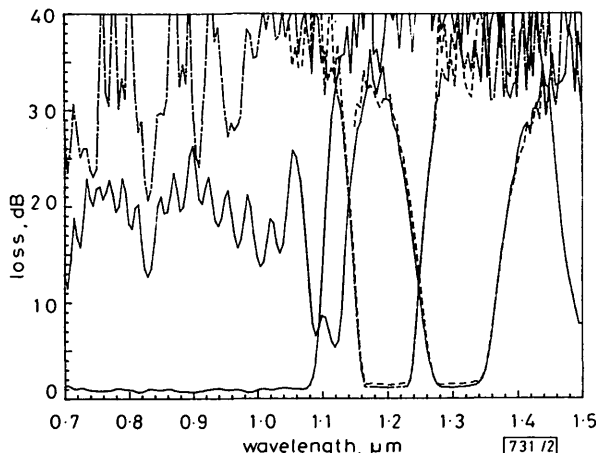


Fig. 2 Wavelength loss characteristics of multi/demultiplexer

Solid lines are for  $\text{CH}_1$  and  $\text{CH}_3$ , broken line with dots is for  $\text{CH}_2$  in demultiplexing. Broken lines are for  $\text{CH}_2$  and  $\text{CH}_3$  in multiplexing

**Characteristics:** The wavelength loss characteristics are shown in Fig. 2. For the DEMUX, the insertion losses were 0.7 dB, 1.1 dB and 1.1 dB for  $\text{CH}_1$ ,  $\text{CH}_2$  and  $\text{CH}_3$ , respectively, before pigtailing (after assembly 1.0 dB, 1.4 dB and 1.3 dB). The 90% transmittance bandwidths were 66 nm and 67 nm for  $\text{CH}_2$  and  $\text{CH}_3$ , respectively, which are wide enough for a WDM transmission system with laser light sources. Far-end crosstalk attenuations were 22–40 dB. If necessary, higher isolation could be achieved by inserting an extra filter in an additional slot. For the MUX, insertion losses were as low as 1.2 dB ( $\text{CH}_1$ ), 1.4 dB ( $\text{CH}_2$ ) and 1.5 dB ( $\text{CH}_3$ ). Near-end crosstalk attenuations, for example when  $\text{CH}_3$  was used as a multiplexing port, were 73 dB and 76 dB for  $\text{CH}_1$  and  $\text{CH}_2$ , respectively. The losses of the MUX/DEMUX are listed in Table 1.

**Conclusion:** The combination of the newly devised filters and the low-loss gradient-index waveguides in glass with a novel geometry including the smaller branching angle resulted in a high-performance guided-wave MUX/DEMUX with low insertion losses and wide transmission bandwidth that conventional designs are unlikely to attain. The MUX studied is well suited for various WDM transmission systems and fibre-

optic sensor systems. A single-mode version of the MUX is now under study.

Table 1 INSERTION LOSS AND FAR-END CROSSTALK ATTENUATION

Output channel	Input signal		
	CH <sub>1</sub>	CH <sub>2</sub>	CH <sub>3</sub>
$\text{CH}_1$	dB 0.7*	dB 1.2	dB >40
	1.2		>40
$\text{CH}_2$	32.8	1.1*	37.9
		1.4	
$\text{CH}_3$	22.0	31.1	1.1*
			1.5

DEMUX insertion loss or far-end crosstalk attenuation

\* MUX insertion loss

**Acknowledgments:** We are grateful to Prof. S.-I. Tanaka of the University of Tokyo for his useful suggestions and encouragement. We also wish to thank Dr. T. Nakajima and Dr. Y. Ikeda for their guidance in the course of the work.

M. SEKI  
R. SUGAWARA  
Y. HANADA  
E. OKUDA  
H. WADA  
T. YAMASAKI

15th July 1987

Tsukuba Research Laboratory  
Nippon Sheet Glass Co., Ltd.  
5-4, Tokodai, Toyosato-Machi, Tukuba-Gun  
Ibaraki Pref. 300-26, Japan

## References

- OKUDA, E., TANAKA, I., and YAMASAKI, T.: 'Planar gradient-index glass waveguide and its applications to a 4 port branched circuit and star coupler', *Appl. Opt.*, 1984, **23**, pp. 1745–1748
- OKUDA, E., WADA, H., and YAMASAKI, T.: 'Planar waveguide 8-port branched circuit'. Technical digest, 7th topical meeting on integrated and guided-wave optics, Florida, 1984, ThB6-1
- OKUDA, E., WADA, H., and YAMASAKI, T.: 'Optical access and star coupler composed of planar gradient-index glass waveguide'. Technical digest, IOOC-ECOC '85, Venezia, pp. 423–426
- TOKURA, N., OIKAWA, Y., and KIMURA, Y.: 'High-reliability 100 Mbit/s optical accessing loop network system: OPALNET-II', *J. Lightwave Technol.*, 1985, **LT-3**, pp. 479–489
- KAWACHI, M., YAMADA, Y., YASU, M., and KOBAYASHI, M.: 'Guided-wave optical wavelength-division multi/demultiplexer using high-silica channel waveguides', *Electron. Lett.*, 1985, **21**, pp. 314–315
- SEKI, M., SUGAWARA, R., OKUDA, E., WADA, H., YAMASAKI, T., and HANADA, Y.: 'Low-loss, guided-wave multi/demultiplexer using embedded gradient-index ion exchange waveguides'. Technical digest, ECOC '86, Barcelona, WD-1
- SEKI, M., SUGAWARA, R., OKUDA, E., HANADA, Y., and YAMASAKI, T.: 'Making a high performance guided-wave multi/demultiplexer by effective design considerations'. Technical digest, OFC/IOOC '87, Reno, TUK2

## GaInAsP/InP UNSTABLE RESONATOR LASERS

*Indexing term: Semiconductor lasers*

Double-heterostructure GaInAsP/InP unstable resonator lasers have been fabricated for the first time. Both facets are made by a simple two-step chemical etching process. The required nearly vertical lateral curved cavity mirrors are achieved. The unstable resonator lasers exhibit an output power of 105 mW.

The unstable resonator GaAs/AlGaAs laser has been studied by several authors.<sup>1–3</sup> Compared with the Fabry-Perot resonant cavity, the unstable resonator suppresses the filamentation

phenomenon in a semiconductor laser. Thus, unstable resonator lasers hold the promise of improved focusing properties and higher coherent output power compared to conventional double heterostructure Fabry-Perot cavity lasers.<sup>4</sup> These characteristics of unstable resonator lasers are very advantageous for GaInAsP/InP lasers with wavelengths between 1.3 and 1.5  $\mu\text{m}$ . Until recently, GaInAsP/InP lasers have been mostly fabricated using the liquid phase epitaxy (LPE) technique. The LPE-grown wafers are much less uniform than MBE AlGaAs/GaAs wafers, so the filamentation problem is even more serious in GaInAsP/InP lasers. The realisation of an unstable resonator laser in this material system which fulfills the theoretical prediction is of substantial interest.

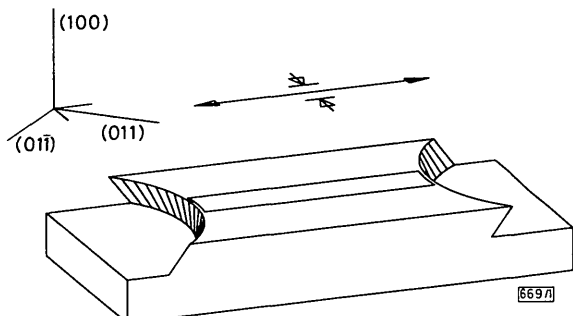


Fig. 1 Schematic drawing of InP/GaInAsP unstable resonator laser with wet-etched curved facets

Crystallographic orientation of resonator is shown;  $W = 58 \mu\text{m}$ ,  $L = 315 \mu\text{m}$ ,  $R = 200 \mu\text{m}$

Fig. 1 shows a schematic drawing and the geometry of the GaInAsP/InP unstable resonator laser. The multilayer structure is that of a conventional DH laser<sup>5</sup> with an active layer 1000 Å thick. The lateral width of the gain region is defined by a 58  $\mu\text{m}$  contact stripe. The radius of curvature of the mirrors is  $R = 200 \mu\text{m}$  and the length of the laser is 315  $\mu\text{m}$ , which correspond to a magnification factor of 5 and an equivalent Fresnel number of 25.<sup>6</sup> Higher magnification factors are more effective in suppressing filamentation, but they also increase the threshold current. Our experiments with a higher ( $M = 6.2$ ) and a lower ( $M = 3.7$ ) magnification factor led to inferior performance.

GaInAsP/InP double heterostructures were grown by conventional liquid phase epitaxy. To etch a vertical mirror, the anisotropic etching characteristics of InP and GaInAsP must be accounted for. When etched in HCl, InP has two etching profiles of opposite slope along the (011) and (011̄) directions so the etching profile in the intermediate diagonal direction should exhibit a vertical slope. With the mirror oriented at 45° with respect to (011) and (011̄), the bisector of

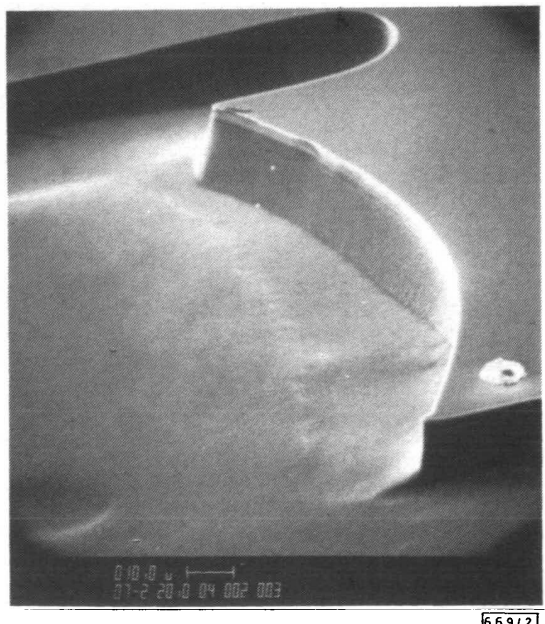


Fig. 2 Scanning electron microscope photograph of etched unstable resonator mirror

these two cleaving directions, the etching was performed at a temperature of 5°C using HCl and an HCl:acetic acid :  $\text{H}_2\text{O}_2$  (15 : 4 : 1) solution for InP and GaInAsP, respectively. By using this approach, nearly vertical walls were obtained (Fig. 2). Using photoresist as the etching mask, this technique of mirror etching is reproducible and reliable. For the unstable resonator lasers, the curvature of the mirrors induces a slight deviation from verticality. When using this etching technique, the vertical slant angle will be approximately equal to the lateral angle with respect to the above-mentioned bisector, limiting it in our design to about 8°.

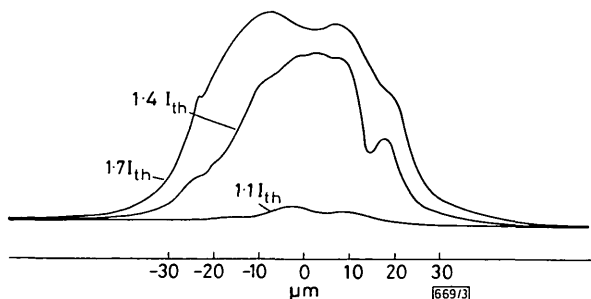


Fig. 3 Near-field intensity distribution of unstable resonator laser at different injection current levels

Fig. 3 shows the near-field pattern of the unstable resonator laser at different injection current levels. The lateral field distribution is stable, but the full width at half-maximum (FWHM) of the output (40  $\mu\text{m}$ ) is less than the metallisation width (58  $\mu\text{m}$ ), probably due to the deviation of the mirror from the ideal vertical position near the edges. Our simple estimate shows that over the 'working' part of the facet, the deviation from the verticality is less than 5.7°. The virtual source point<sup>4</sup> is predicted to be 47  $\mu\text{m}$  behind the laser facet, in fair agreement with the measurement. In Fig. 4 we show the far-field pattern of the same laser. The far-field angle is quite wide, as expected. The lasers have a typical threshold current of 1.4–1.6 A and an output power of about 105 mW.

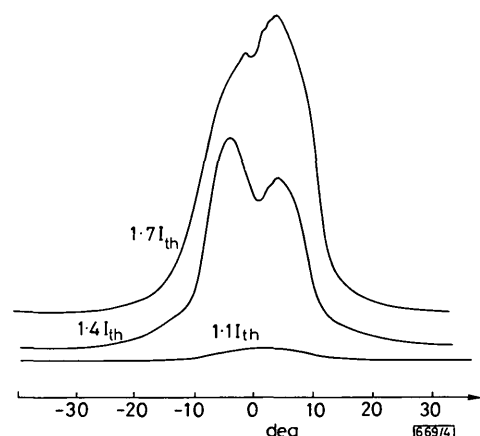


Fig. 4 Far-field intensity distribution of unstable resonator laser at different injection current levels

In conclusion, a convenient chemical facet etching method has been developed, and a GaInAsP/InP unstable resonator laser has been demonstrated for the first time. An output power of 105 mW from each facet was measured. The measured characteristics of the laser beam are in good agreement with theoretical predictions. The InP/GaInAsP unstable resonator laser is a promising optical source for optical long-distance communications.

The support of the Office of Naval Research and of the Army Research Office is gratefully acknowledged.

H. WANG  
Y. Y. LIU  
M. MITTELSTEIN  
T. R. CHEN  
A. YARIV

California Institute of Technology  
Pasadena, CA 91125, USA

6th July 1987

## References

- 1 BOGATOV, A. P., ELISEEV, P. G., MANKO, M. A., MILAELYAN, G. T., and POPOV, Y. M.: 'Injection laser with an unstable resonator', *Sov. J. Quantum Electron.*, 1980, **10**, pp. 620-622
- 2 CRAIG, R. R., CASPERSON, L. W., STAFSUDD, O. M., YANG, J. J. J., EVANS, G. A., and DAVIDHEISER, R. A.: 'Etched-mirror unstable-resonator semiconductor lasers', *Electron. Lett.*, 1985, **21**, pp. 62-63
- 3 SALZMAN, J., VENKATESAN, T., LANG, R., MITTELESTEIN, M., and YARIV, A.: 'Unstable resonator cavity semiconductor lasers', *Appl. Phys. Lett.*, 1985, **46**, pp. 218-220
- 4 MITTELESTEIN, M., SALZMAN, J., VENKATESAN, T., LANG, R., and YARIV, A.: 'Coherence and focusing properties of unstable resonator semiconductor lasers', *ibid.*, 1985, **46**, pp. 923-925
- 5 CHEN, T. R., YU, K. L., CHANG, R., HASSON, A., MARGALIT, S., and YARIV, A.: 'Phase locked InGaAsP laser array with diffraction coupling', *ibid.*, 1983, **43**, pp. 136-137
- 6 SIEGMAN, A. E.: 'Unstable optical resonator for laser applications', *Proc. IEEE*, 1965, **53**, pp. 277-287

## WIDEBAND MONOLITHIC GaAs AMPLIFIER USING CASCODES

*Indexing term: Amplifiers*

A monolithic matched, two-stage wideband amplifier with an insertion gain of 26 dB and a -3 dB bandwidth of 3.2 GHz is reported. Optimally designed cascode circuits are used to enhance the gain-bandwidth product available per stage. The IC has been fabricated in a 1  $\mu\text{m}$  depletion GaAs MESFET technology.

**Introduction:** There is a continuing demand for DC coupled wideband amplifiers in microwave communication systems, fibre optics amplifiers and instrumentation. Several Si<sup>1,2</sup> and GaAs<sup>3</sup> monolithic amplifier designs have been reported recently. Most of the GaAs circuits derive from a shunt feed-

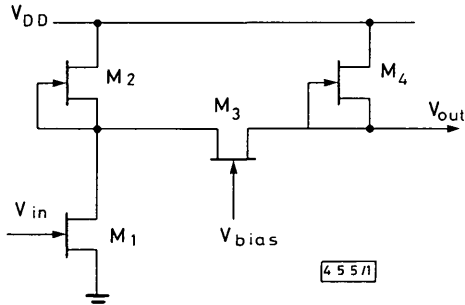


Fig. 1 MESFET cascode amplifier circuit

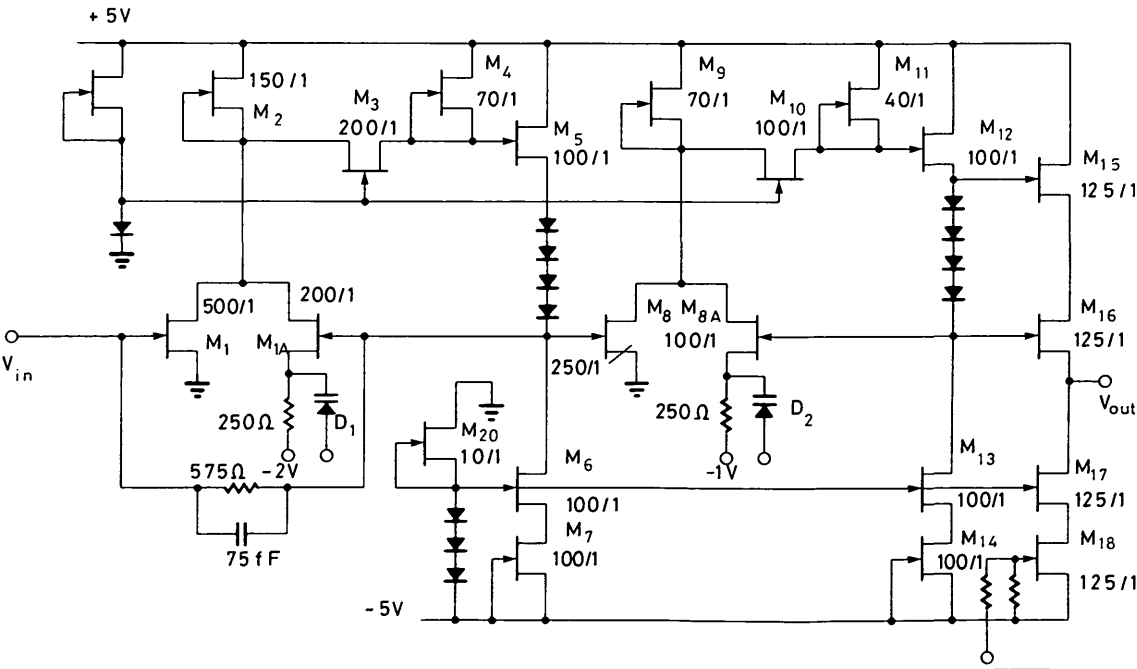


Fig. 2 Schematic diagram of complete wideband amplifier

back topology<sup>4</sup> that is well proven in the robustness of its bias point and gain against processing variations. However, the gain-bandwidth product available per stage is limited, which, in turn, limits the gain of the overall amplifier. Thus, the gain of the GaAs amplifier referenced above<sup>3</sup> was 22 dB, with a bandwidth of 2.5 GHz.

We describe here an amplifier that, using improved design techniques, is capable of a 26 dB gain with a bandwidth of 3.2 GHz, when fabricated in a comparable technology.

**Features of circuit design:** The key to improved gain and bandwidth for a feedback amplifier is to use individual stages with a high gain-bandwidth product. For a given technology, this product may be enhanced by cascading two or more stages, and applying overall feedback around them. Simple feedback requires that the cascade has an inverting transfer function to obtain negative feedback in the loop. Thus, in a straightforward cascade, at least three inverting gain stages must be used. The limitation of this scheme is that the phase lag through three stages can accumulate sufficiently at high frequencies to produce instability in the feedback loop.

The cascode circuit (Fig. 1) offers an inverting cascade of two stages. By ratioing the sizes of devices M<sub>2</sub> and M<sub>3</sub>, an overall gain approximately equal to the product of the gains of two common-source stages may be obtained. In our circuit this gain was designed to be about 25 dB. The phase lag through this configuration is also always less than that through three stages. A high bandwidth after feedback may be obtained because the three important poles, namely those at the gate of M<sub>1</sub>, at the drain of M<sub>1</sub> and at the drain of M<sub>3</sub>, may all be made comparable to each other in frequency, so that no one pole dominates. The closed-loop poles will then be complex, and may be adjusted to provide a maximally flat response.

Our two-stage amplifier (Fig. 2) consists of a trans-impedance stage to match the input impedance to 50  $\Omega$ , followed by a second stage to drive a 50  $\Omega$  load. Each stage has local feedback provided by a shunt feedback FET (transistors M<sub>1A</sub> and M<sub>8A</sub>). A unique feature of this design is the presence of the RC degeneration network at the sources of these FETs. This network provides controllable peaking at the band edge of the amplifier. The amount of peaking can be changed by varying the reverse bias across Schottky diodes D<sub>1</sub> and D<sub>2</sub>. This technique may be understood as follows. At high frequencies, the phase lag through the feedback loop can become so large that, if M<sub>1A</sub> has a grounded source, I<sub>D</sub>(M<sub>1A</sub>) may become in phase with I<sub>D</sub>(M<sub>1</sub>), thus producing excessive peaking in the frequency response. The degeneration network acts to make I<sub>D</sub>(M<sub>1A</sub>) = j $\omega$ C<sub>V</sub>(M<sub>1A</sub>), thus introducing a 90° phase lead to counteract the phase lag. This reduces the peaking to a small and controllable amount.